Efficient processing method for material card definition of AHSS and UHSS to predict fracture in crash analysis and its application to vehicle crash model

Kang Hee Lee[1], Dae Young Kim[1], Chul Woong Jun[2], Kyoung Teak Lee[2]

[1]Hyundai Steel R&D Center
[2]Korea Simulation Technologies[KOSTECH]

1 Abstract

Crashworthiness of the vehicle body is getting importance to meet the enhancing vehicle crash safety regulations. To improve the vehicle body crashworthiness, application of Advanced high-strength steels (AHSS) and Ultra high-strength steels (UHSS) are continuously increasing due to their superior strength than conventional high-strength steels (HSS). However due to the lower ductility of AHSS and UHSS, material fracture can occur during crash scenario and it affects the overall performance of vehicle. To prevent this problem, CAE tool has important role in design stage of the vehicle body. CAE material model is steadily increasing and many fracture models are developed to predict the material fracture phenomena in crash scenario. Especially, Generalized incremental stress state dependent model (GISSMO) is widely used to predict the material fracture in crash scenario. Material card for crash simulation needs plasticity curves at various strain rates to predict the material behavior at high speed deformation and GISSMO parameter to predict the material behavior at high amount of local deformation. However, due to many parameters and data has to be defined for each material cards, the definition process is very complicated and time consuming. So, efficient processing method is required to effectively define material cards for various steel grades applied to vehicle body structure.

In this study, a user interface program is developed and verified to efficiently process the material card definition for crash analysis. LS-OPT and LS-DYNA linked calculation method included in this process helps to define material cards with reliable and effective results. Material cards for AHSS and UHSS for vehicle body structure were defined and verified. 5 Types of coupon test specimens and some component test specimens were used. Finally, material cards were introduced in H-Solution EV concept vehicle model which developed by Hyundai-Steel and 3 crash load cases were implemented. Analysis result of 2 types of vehicle crash model which introduce different material grades for the major body parts help to evaluate the crashworthiness result of each material grades and helps to predict the material behavior in vehicle body crash scenario. According to this study, it can be shown that the material card for crash analysis can be efficiently defined with the process and helps to predict the performance of the vehicle body structure by applying it into crash scenario model.

2 Material evaluation and modeling for vehicle crash analysis

Steel usually accounts for the highest proportion of car body material. Mild steel is mainly applied to exterior panels. Advanced High Strength Steel(AHSS) and Ultra High Strength Steel(UHSS) are applied to structure parts. The severity of crash tests provided by evaluation agencies such as IIHS, NHTSA and EURO NCAP is also trending to become more stringent. In order to improve the vehicle's crash performance in line with the strengthened crash regulations, the application ratio and strength of the AHSS and UHSS are both has been increasing in car body. Accordingly, evaluation of the material characteristics of has become important, and many research is being conducted on the evaluation method for dynamic behavior and fracture of AHSS & UHSS [1, 2]. The crash performance of the car body can be evaluated analytically through CAE. In order to predict the crash behavior of the car body more accurately through CAE, it is necessary to use accurate material card based on the test result with dynamic effect and fracture property.

2.1 Plasticity with strain rate

In order to analyze the crash performance of vehicles, plasticity with strain rate of the applied material are generally used [3]. During material deformation in a crash scenario, deformation occurs at high speed. At this time, since the energy absorbed by the body member changes while the behavior of the material changes according to the applied strain rate, the strain rate effect should be considered.

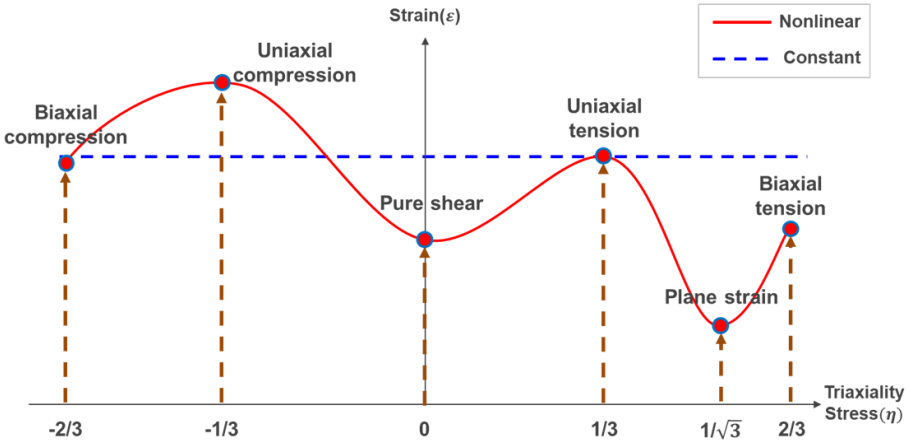

Fig.1: Fracture strain in various stress state.

2.2 GISSMO

Recently, the application of AHSS and UHSS is steadily increasing. As a result, the issue of brittle fracture has emerged. This is because steel has a characteristic in which ductility decreases as strength increases. Various prediction models are being studied to predict the occurrence of such fractures [4, 5]. Also, application cases in the crash field are also increasing. Among them, Generalized Incremental Stress State dependent damage Model (GISSMO) is widely used in automotive crash and forming CAE application [6, 7, 8]. The model considers various factors affecting fracture, and applied together with various constitutive. In GISSMO, the damage is accumulated with the damage increment ΔD as in Equation (1). N is damage exponent and $\Delta\varepsilon_P$ is plastic strain increment where $\varepsilon_f(\eta)$ is a fracture strain which is a function of stress triaxiality.

$$\Delta D = \frac{N}{\varepsilon_f(\eta)} D^{(1-\frac{1}{N})} \Delta\varepsilon_P \tag{1}$$

Stress triaxiality (η), which express the stress state with non-dimensinal value is a function of the hydrostatic stress (σ_h) and the equivalent Von-Mises stress (σ_v) as in Equation (2).

$$\eta = \frac{\sigma_h}{\sigma_v} \tag{2}$$

Since the traditional fracture prediction method was only based on the fracture strain obtained from uniaxial tensile mode. There are limitations in accurately predicting material fracture in the case of vehicle crash scenario where various loads are applied. To improve the reliability of material fracture prediction, stree triaxiality considering various stress states had been introduced. (Figure 1) GISSMO also introduces an instability indicator F, as shown in Equation (3) to determine the onset of material softening.

$$\Delta F = \frac{N}{\varepsilon_{ins}(\eta)} F^{(1-\frac{1}{N})} \Delta\varepsilon_P \tag{3}$$

Where, ΔF is the instability indicator increment, N is damage exponent also applied in Equation (1) and $\varepsilon_{ins}(\eta)$, which is a function of stress triaxiality is equivalent plastic strain at the onset of instability.

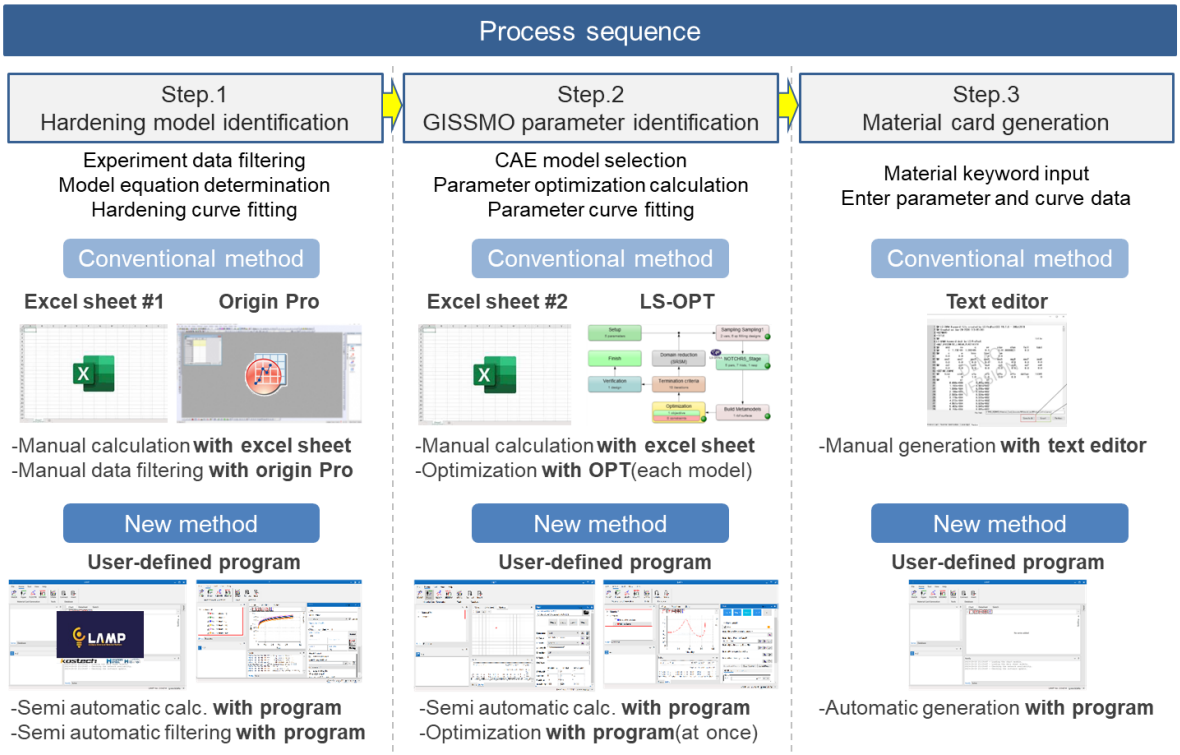

Fig.2: Overall process of material card definition for crash analysis.

Stress is updated by the damage accumulated by the damage increment in Equation (1). D_{crit} is damage at the critical point of the instability indicator and m is the fading exponent (FADEXP) which determines the degree of stress reduction.

$$\sigma^* = \sigma[1 - \left(\frac{D - D_{crit}}{D_{crit}}\right)^m] \quad (D \geq D_{crit}) \tag{4}$$

3 Process for material card definition (with user-defined program)

3.1 Overall process

Overall process of material card definition for crash application and its processing methods are shown in Figure 2. The entire process can be divided into 3 steps with Hardening curve identification, GISSMO parameter identification and Material card generation. In Step 1, experimental data filtering and hardening model determination are performed. In Step 2, the optimal value of each parameter is determined to define the GISSMO parameters and parameter curve fitting is performed. Finally, in Step 3, the parameters determined in the previous step are entered into each material keyword to complete the material card.

But the conventional processing method for this process was very complicated and time-consuming because repetitive manual work was accompanied by going back and forth between multiple programs such as excel spread sheet calculation, LS-OPT and text editor. For dynamic hardening curve identification, the parameters for the plasticity equation parameter and rate effect term must be determined. In addition, for GISSMO parameter identification, there are many parameters such as DMGEXP, FADEXP, $\varepsilon_f(\eta)$ and $\varepsilon_{ins}(\eta)$ that must be determined, as introduced in 2.2.
With curve data parameters, the whole process become more complicated because curve fitting through model equation is also required.

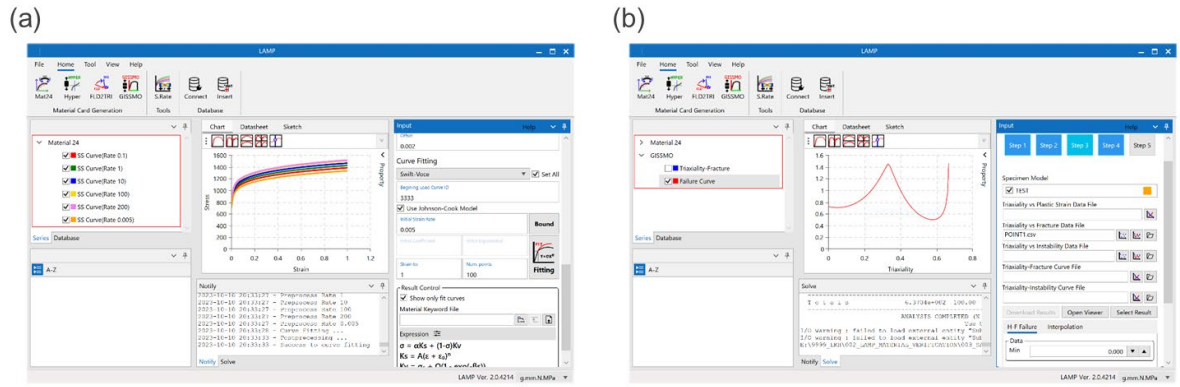

Fig.3: Developed user-defined program for crash material card definition.

For more efficient processing that overcomes the difficulties of conventional methods, we designed a user-defined program that can perform all steps in a single program. The user-defined program co-developed by Hyundai-Steel R&D Center and KOSTECH is based on C++language. The program contains all functions necessary for these material card definition process. Program functions include preprocessing of experiment data, model equation fitting, parameter optimization through LS-OPT automatic linkage calculation, optimization result table configuration and automatic material card generation. By carrying out all these complex process in a single program, the material card definition process for crash application can be time-efficient, simple and standardized compared with conventional processing method.

In this study, 3 types of steel were presented as representative crash material cards of advanced high-strength steel derived through a user-defined program. The details of each step are explained in the following headings.

3.2 Experiment data and CAE specimen model

To calibrate the hardening curve considering the strain rate effect, experiment data for six strain rates of 0.005, 0.1, 1, 10, 100, and 200/s were obtained using the high rate tensile test machine.
For GISSMO parameter calibration, five types of specimens were used for each deformation mode and test data for 10/s rate were obtained as representative data. When comparing the effect on the test rate for each deformation mode, some studies reported that the change in fracture strain according to the strain rate in tension, notch tension, and biaxial tension is relatively small, but the effect in shear deformation mode is not negligible [9].

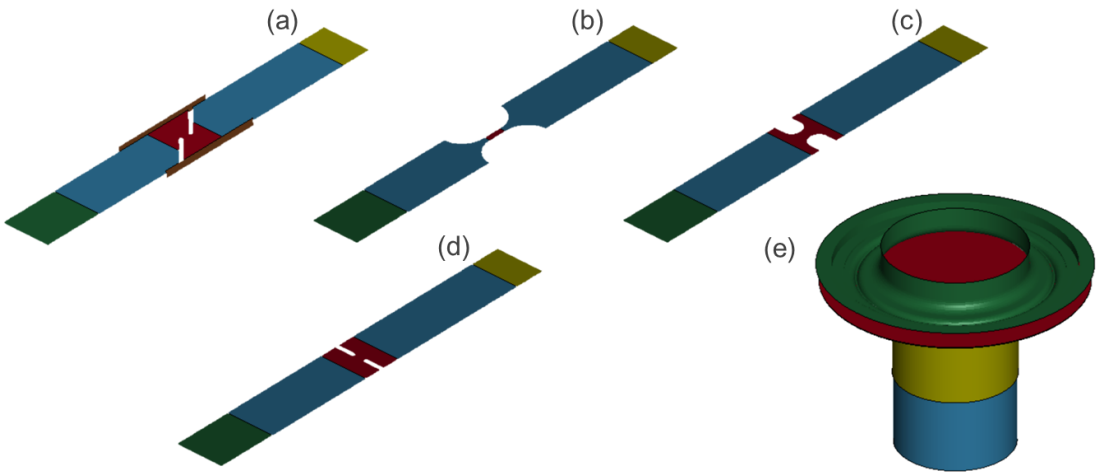

Fig.4: CAE specimen model. (a) Simple shear (b) Uniaxial tension (c) Notched tension R5 (d) Notched tension R1 (e) Biaxial tension

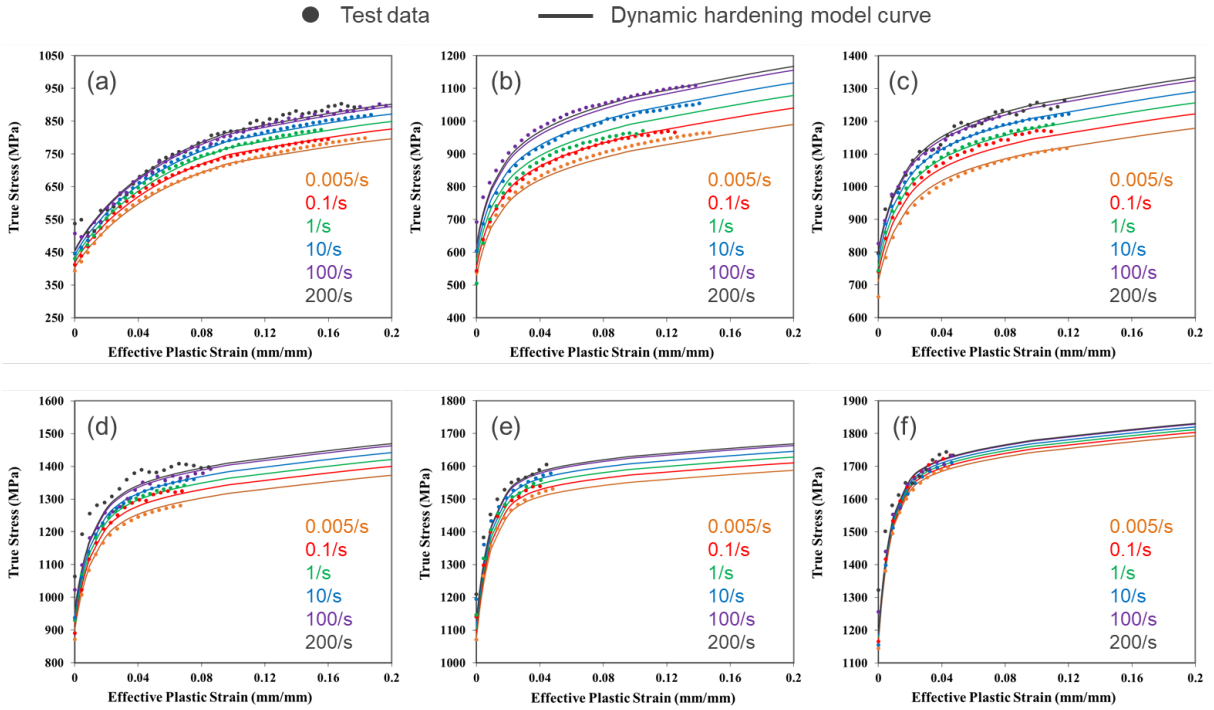

Fig.5: Dynamic hardening curve for AHSS and UHSS. (a) 600MPa CR (b) 800MPa CR (c) 1.0GPa CR (d) 1.2GPa CR (e) 1.5GPa PHS (type1) (f) 1.5GPa PHS (type2)

However, since the CAE crash model applied in this study is mainly involved in the region where stress triaxiality value is given above the uniaxial tensile region (ie, stress triaxiality value above 0.33), the fracture strain change in shear mode with deformation rate was not considered. The crash material card considering the deformation rate effect will be applied after additional verification as a future work.

In the case of the shear specimen among the five specimens, rotation of the specimen occurs during deformation, it is difficult to maintain the simple shear mode until the point of fracture without additional constrain. So in the case of the shear specimen used in this study, a guide jig was used to maintain a simple shear mode (i.e., stress triaxiality value 0). As a result, it can be confirmed that the simple shear mode is well maintained until the point of fracture by preventing the rotation of the specimen.

As input data, the load vs displacement experiment data file and CAE model file for each specimen were applied, and subsequent processes were performed by inputting them into a user-defined program. 3 type of steel grade (1.0GPa CR, 1.5GPa PHS type1 and type2) and their data are used in this process.

3.3 Dynamic hardening model calibration

To determine the dynamic hardening model considering strain rate effect, Mixed Swift-Voce model was applied with Johnson Cook type rate term.

$$\overline{\sigma}(\overline{\varepsilon}_p, \dot{\overline{\varepsilon}}_p) = \overline{\sigma}(\overline{\varepsilon}_p) * \overline{\sigma}(\dot{\overline{\varepsilon}}_p) \tag{5}$$

$$\overline{\sigma}(\overline{\varepsilon}_p) = \alpha\overline{\sigma}_s(\overline{\varepsilon}_p) * (1-\alpha)\overline{\sigma}_v(\overline{\varepsilon}_p) \tag{6}$$

$$\overline{\sigma}_s(\overline{\varepsilon}_p) = \alpha\{A(\overline{\varepsilon}_p + \varepsilon_0)^n\} \tag{7}$$

$$\overline{\sigma}_v(\overline{\varepsilon}_p) = \sigma_0 + Q\{1 - \exp(-\beta\overline{\varepsilon}_p)\} \tag{8}$$

$$\overline{\sigma}(\dot{\overline{\varepsilon}}_p) = 1 \ \ (\text{for } \dot{\overline{\varepsilon}}_p < \dot{\varepsilon}_0) \ \ \& \ \ 1 + C\ln\left(\frac{\dot{\overline{\varepsilon}}_p}{\dot{\varepsilon}_0}\right) \ \ (\text{for } \dot{\overline{\varepsilon}}_p > \dot{\varepsilon}_0) \tag{9}$$

According to Equation (5), six parameters must be determined. n represents swift type parameter, Q and β for voce type parameters, α for coefficient of mixed Swift-Voce model and C for strain rate coefficient. Also, σ_0 represents yield strength, ε_0 for elastic strain and $\dot{\varepsilon}_0$ for reference strain rate. Applying the corresponding dynamic hardening model for each AHSS and UHSS, similar trends to the experiment data can be confirmed for various grades as shown in Figure 5. In this study, dynamic hardening model for 3 types of steel grades which include 1.0GPa CR, 1.5GPa PHS type1 and 1.5GPa PHS type2 were used in the crash material card definition process.

In the program, the dynamic hardening model calibration process mentioned above was performed by selecting the type of model equation in the extrapolation function menu after loading the experiment base data file.

3.4 GISSMO parameter optimization and curve fitting

Optimization calculations using LS-OPT were performed to determine GISSMO parameters. Optimization was performed for four parameters: DMGEXP, FADEXP, failure strain, and instability strain. A fixed value of 2.0 was used for DMGEXP, and the optimal FADEXP value was first derived based on the uniaxial tension specimen model. Afterwards, the optimal values of failure strain and instability strain were derived for each of the five deformation mode specimen models. Afterwards, curve fitting was performed to interpolate the values for the mid-range other than each point of the representative deformation mode specimen. The Hosford coulomb fracture initiation model (Equation 10) was applied to derive the failure strain curve for entire triaxiality range [10].

$$\bar{\bar{\varepsilon}}_f = b\left(\frac{1+c}{g_{HC}}\right)^{\frac{1}{n}} \tag{10}$$

$$g_{HC} = \left(\frac{1}{2}|f_1 - f_2|^a + \frac{1}{2}|f_2 - f_3|^a + \frac{1}{2}|f_1 - f_3|^a\right)^{\frac{1}{a}} + c(2\eta + f_1 + f_2) \tag{11}$$

$$f_1[\bar{\theta}] = \frac{2}{3}\cos\left[\frac{\pi}{6}(1-\bar{\theta})\right],\ f_2[\bar{\theta}] = \frac{2}{3}\cos\left[\frac{\pi}{6}(3+\bar{\theta})\right],\ f_3[\bar{\theta}] = -\frac{2}{3}\cos\left[\frac{\pi}{6}(1+\bar{\theta})\right] \tag{12}$$

where a, b and c are the parameters. Also n is the hardening index, θ is the lode angle parameter, and η is the stress triaxiality.

$$-\frac{27}{2}\eta\left(\eta^2 - \frac{1}{3}\right) = \sin\left(\frac{\pi}{2}\bar{\theta}\right) \tag{13}$$

In the case of thin plates, a plane stress state can be assumed. Therefore, stress triaxiality and lode angle parameter have the relationship of Equation (13). Polynomial type function was applied to derive the instability strain for the entire triaxiality range. The optimization history for representative specimen and resulting parameter curves for 1.0GPa CR, 1.5GPa PHS type1 and type2 are shown in Figure 6.

In the program, parameter optimization process mentioned above was performed by entering the optimization range of each parameter for all deformation mode specimen model at once. After determining the parameter FADEXP, sequential optimization calculations can be performed automatically for each model to determine the ε_f and ε_{ins}. Once the calculations for all specimen models were completed, the optimization results could be checked at once. Afterwards, interpolation was applied based on the corresponding point values of ε_f and ε_{ins}. Then continuous parameter curve data was derived.

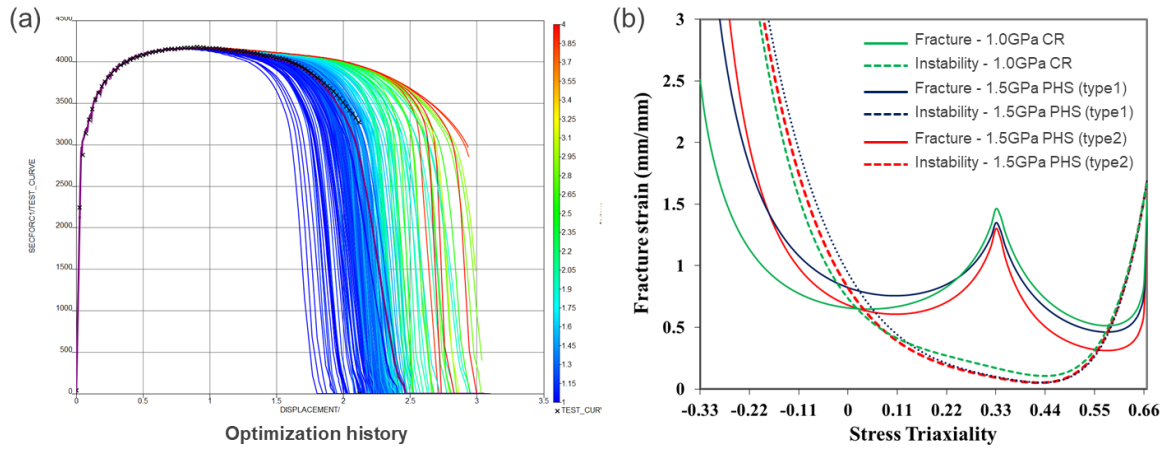

Fig.6: Optimization with LS-OPT and parameter curve. (a) Optimization history (b) Fracture curve & Instability curve

3.5 Element regularization and curve fitting

The optimal GISSMO parameter derived previously is a result based on the element size of 0.5mm. But mesh size small as 0.5mm are rarely used in industry. Generally, element size far larger than 0.5mm are used in vehicle body model due to computation time. Therefore, element size regularization is necessary for application to vehicle crash analysis so that the material behavior can be implemented similarly regardless of element size of the FE model. The optimal value of regularization factor was derived based on the uniaxial tension model application. The FE model element size of 0.4mm, 0.5mm, 0.8mm, 1.5mm and 3.0mm were used. After determining the optimal value for each element size, an exponential type function was applied for interpolation of intermediate values and extrapolation of external values.

$$R = aE_S{}^m \tag{14}$$

where, a and m are the parameters. Also, R is regularization factor and E_S is element size.
The optimization history for representative specimen and resulting parameter curves for 1.0GPa CR, 1.5GPa PHS type1 and type2 are shown in Figure 7.

In the program, parameter optimization process mentioned above was performed by entering the optimization range of each parameter for each element size model at once. Sequential optimization calculation can be performed automatically. Afterwards, an exponential type function was applied based on the point data. Then continuous parameter curve for scale factor was derived.

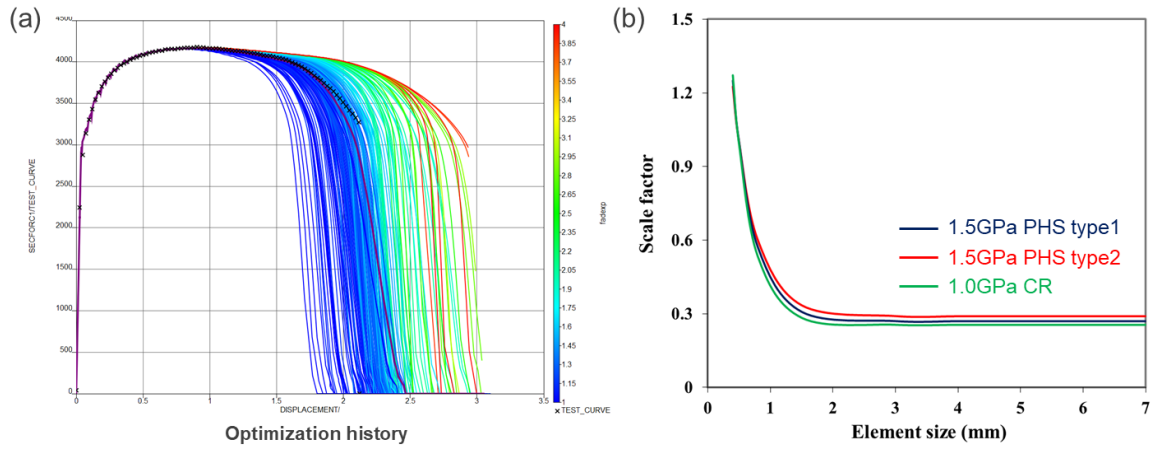

Fig.7: Element regularization scale factor curve. (a) Optimization history (b) Scale factor curve

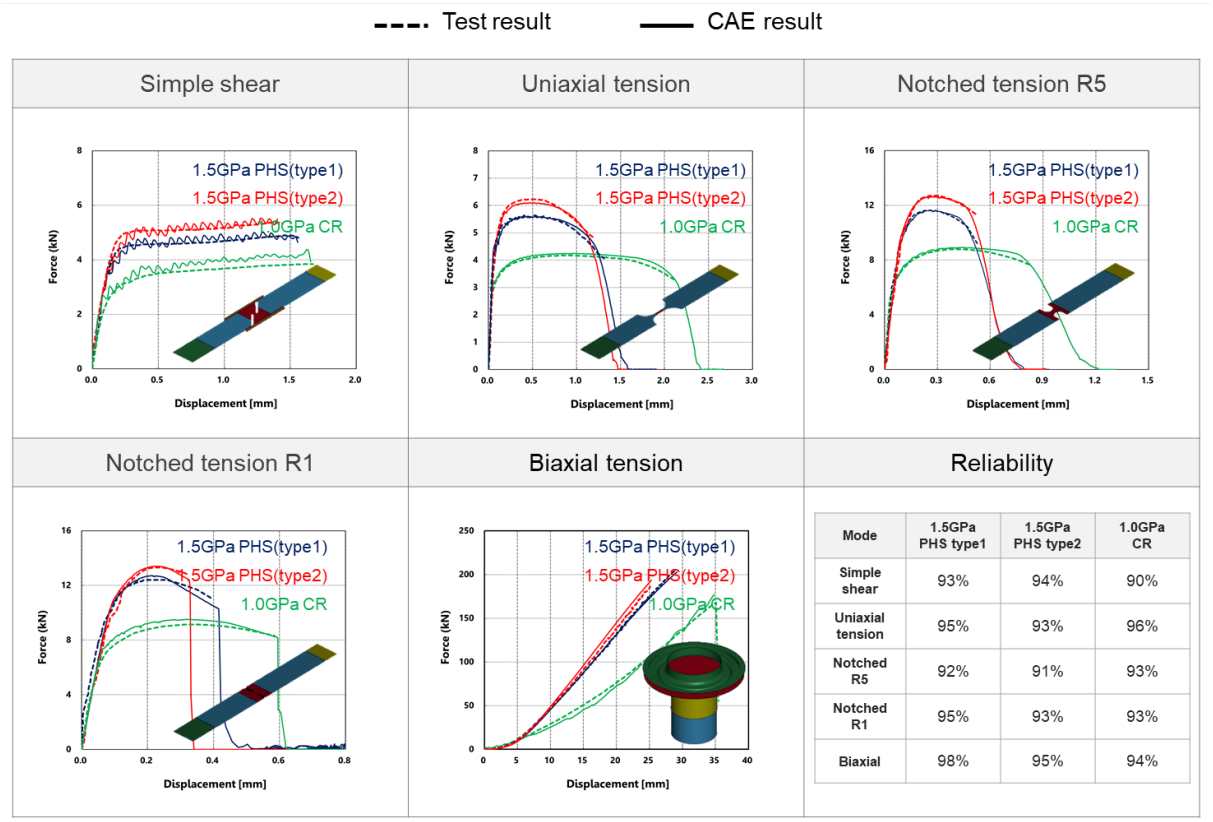

Mode	1.5GPa PHS type1	1.5GPa PHS type2	1.0GPa CR
Simple shear	93%	94%	90%
Uniaxial tension	95%	93%	96%
Notched R5	92%	91%	93%
Notched R1	95%	93%	93%
Biaxial	98%	95%	94%

Fig.8: Validation result with specimen model

3.6 Validation with specimen model

The optimal GISSMO parameters derived in the process up to 3.5 were applied to the entire specimen CAE model. When comparing the load vs. displacement diagram in the test values and CAE results (Figure 8), more than 90% reliability was obtained for both 1.0GPa CR and 1.5GPa PHS type 1 & type 2. Thus, it was confirmed that the derived optimal parameters were valid in the coupon test scale model.

4 Validation with component model

The derived crash material card was verified on a larger scale CAE model through drop weight impact analysis of the omega shape specimen model. UHSSs are mainly applied to body parts that are deformed under bending impact mode during vehicle crash. Therefore, the drop weight impact test was conducted by placing an omega-shaped specimen on a roller support and then applying a crash load with an impactor to the center of the specimen to implement a bending crash mode. (Figure 9)
The CAE model consisted of an average shell element size of 3.0mm. The element formulation type 16 and the shell control option istupd 4 was used.

Due to the imperfection of the test specimen compared to the CAE model, the Energy-Deformation curve at the latter stage of deformation had some differences from the test results. However, it can be seen that the overall energy response and maximum deformation value were predicted similarly.
Additionally, it can be seen that the crack location and crack length in the test are similar to the eroded elements and eroded area in the CAE model. This shows that the overall crash deformation behavior, including fracture occurrence, was well predicted. Through this, the consistency of the derived crash material card could be confirmed in a larger scale component level CAE model.

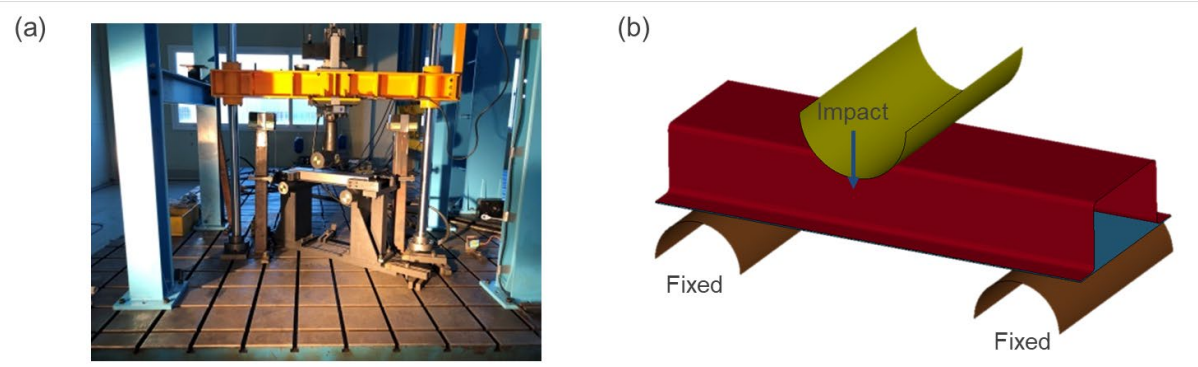

Fig.9: Bending crash configuration. (a) Test equipment (b) CAE model

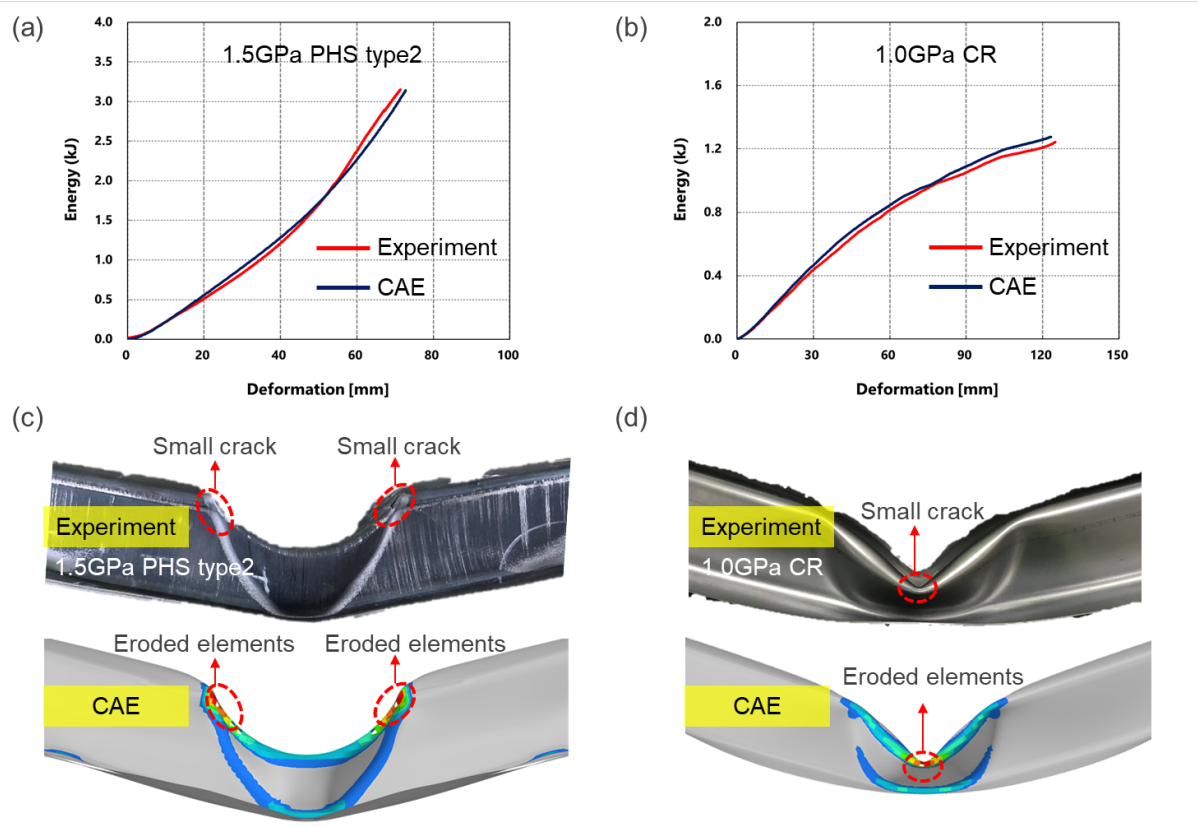

Fig.10: Bending crash analysis result. (a) Energy-Deformation curve for 1.5GPa PHS type2 (b) Energy-Deformation curve for 1.0GPa CR (c) Post crash specimen and CAE result for 1.5GPa PHS type2 (d) Post crash specimen and CAE result for 1.0GPa CR

5 Application to vehicle crash model

The crash material card derived through the material card definition procedure using the user defined program was applied to FE crash simulation using a full vehicle model.

The full vehicle model used in crash simulation is the H-solution EV 1st concept body model developed in-house by Hyundai Steel. It was first unveiled at the 2019 Shanghai Motor Show, and steel types developed in-house by Hyundai Steel were applied to major body parts. The material ratio within the body in white application is shown in Figure11. It is characterized by a high ratio of UHSS and AHSS, including press hardened steel parts.

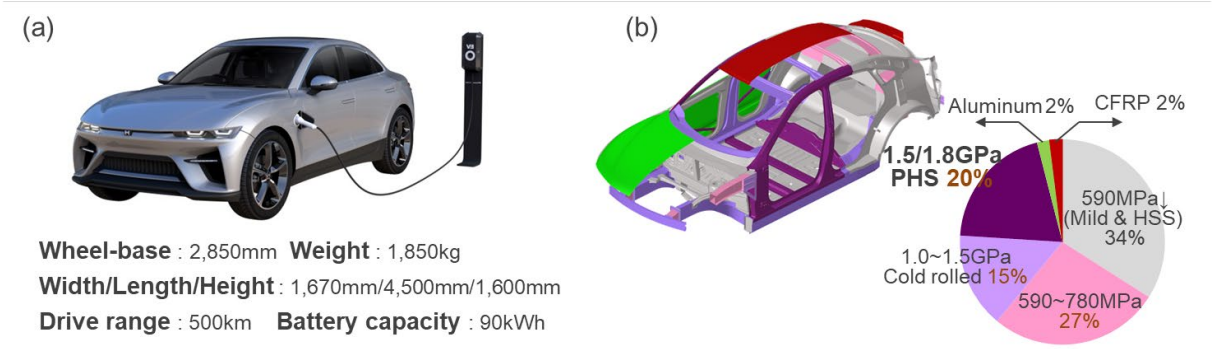

Fig.11: Hyundai-Steel H-Solution 1st EV concept car. (a) Vehicle specification (b) Body-In-White material mix

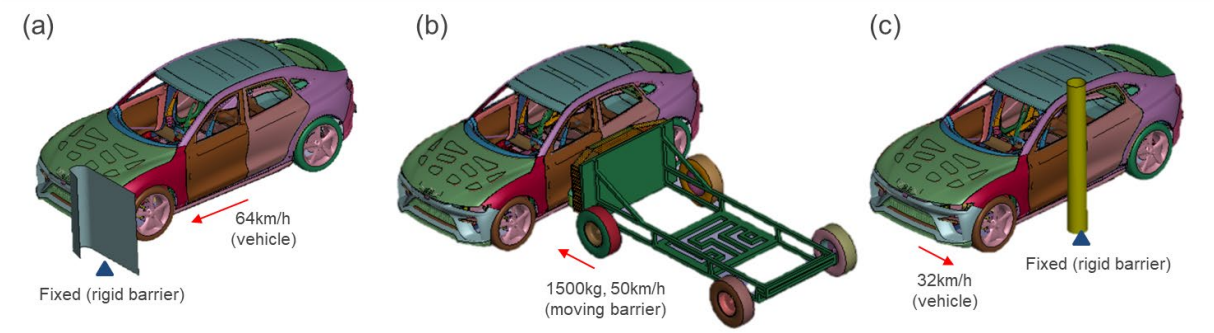

Fig.12: Load cases for vehicle crash analysis with H-Solution EV concept body model (a) Small overlap (b) Side impact (c) Side pole crash

The main crash tests used to evaluate vehicle crash performance can be divided into front crash test, side crash test, and rear crash test modes. The types of frontal crash tests are subdivided into full frontal, moderate overlap, small overlap, and MPDB. Side crash tests can be divided into side impact and side pole crashes. Among these, crash analysis was performed in this study for three crash scenario (Figure 12) : small overlap frontal crash, side impact, and side pole crash, mainly influenced by the 1.0GPa CR and 1.5GPa PHS obtained in the previous crash material card definition process.

Crash analysis result for side impact CAE model are shown in Figure 13. In original side crash test, a moving deformable barrier weighing 1500kg crashes 90 degrees of the vehicle driver direction at a speed of 50km/h.
In Case 2 where 1.5GPa PHS type2 was applied to the B-pillar outer and 1.0GPa CR was applied to the B-pillar inner, element deletion occurred in the main deformation area of the B-pillar as shown in Figure 13(c). Due to bending deformation, high strain was concentrated in local areas, causing fracture of several elements that reached a damage value of 1.0. However, the fracture was small and limited to a local area, the overall intrusion level of the B pillar was higher than 125 mm from the driver seat centerline. It can be confirmed that this falls within the Good level according to the IIHS evaluation standard. On the other hand, in the Case 1 where 1.5GPa type1 was applied to the B-pillar outer and 1.0GPa CR was applied to the B-pillar inner, element deletion did not occur anywhere in the main deformation area of the B-pillar, as shown in Figure 13(b). Although high strain was concentrated in a local area due to bending deformation, the element did not fracture because it did not reach a level that caused damage beyond the fracture limit of the material.
Both Case 1 and Case 2 belongs to the Good level according to the IIHS evaluation standard.

Crash analysis result for side pole CAE model are shown in Figure 14. In side pole crash test, the vehicle crashes into a rigid pole at a speed of 32km/h and the impact reference line angle is 75 degree from the vehicle longitudinal centerline.
In Case 2 where 1.5GPa PHS type2 was applied to the side sill outer, element deletion occurred in the main deformation area as shown in Figure 14(c). On the other hand, in the Case 1 where 1.5GPa PHS

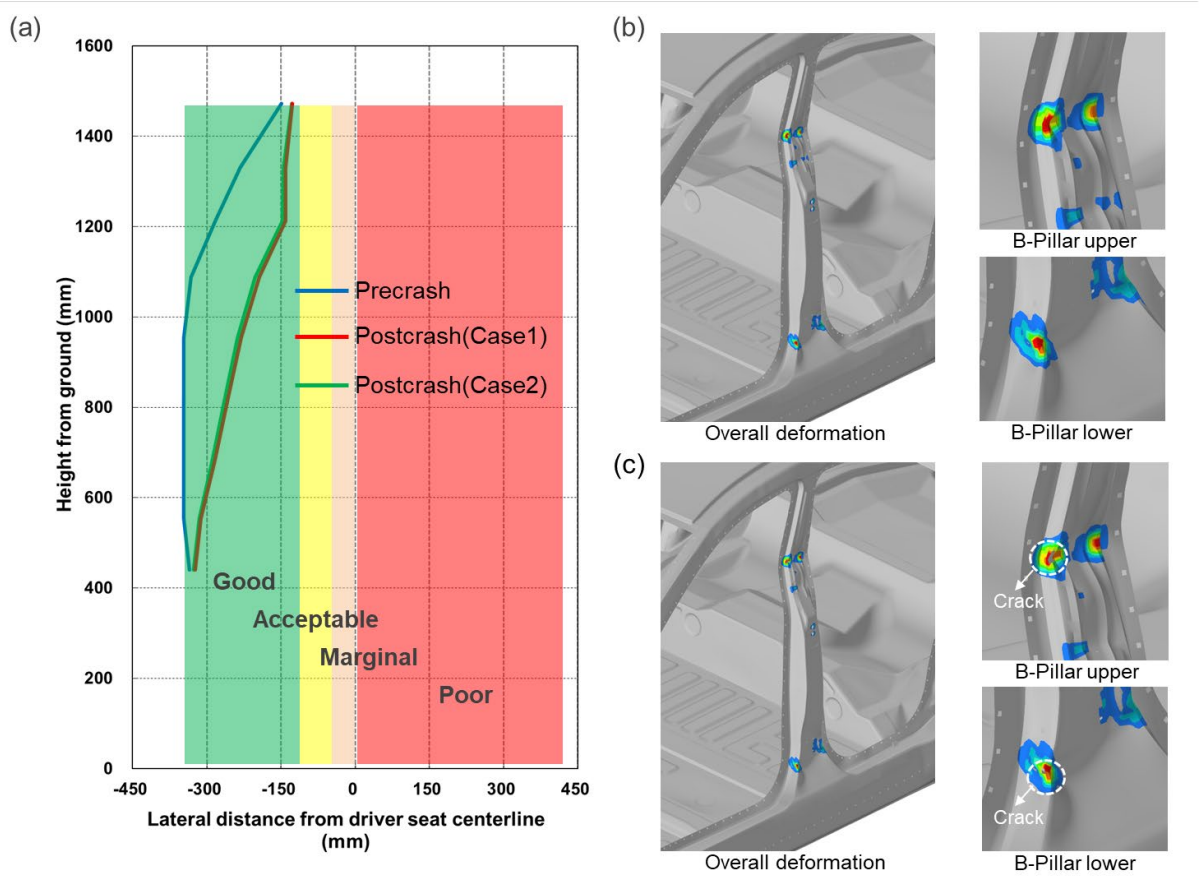

Fig.13: CAE analysis result of side impact. (a) B-Pillar intrusion level (b) B-Pillar deformation(Case1) (c) B-Pillar deformation(Case2)

type1 was applied to the side sill outer, element deletion did not occur anywhere in the deformation area, as shown in Figure 14(b).

Crash analysis result for small overlap crash CAE model are shown in Figure 15. In small overlap crash test, 25% of vehicle width overlaps and crashes into a rigid barrier at speed of 64km/h.
In Case2 where 1.5GPa PHS type2 was applied to A-pillar upper/lower and side sill outer, element deletion occurred in the front part of the side sill and lower part of the A-pillar. Due to its harsh condition of small overlap, high crash energy concentrate into local part of the vehicle, complex deformation concentrate in the local area cause fracture of several elements. In Case1 where 1.5GPa PHS type1 was applied in the same part, also element erosion occurred but to a lower degree than Case2. Both Case 1 and Case 2, the overall intrusion level of lower and upper occupant compartment belongs to the Good level according to the IIHS evaluation standard.

As a result of applying the crash material card derived through the process of this study to car body crash analysis, it was predicted that the crash safety performance of the car body could be secured by applying the 1.5GPa and 1.0GPa grades to major crash compartment. In addition, it was predicted from the vehicle crash analysis results that among similar 1.5GPa PHS materials, if the fracture curve value is higher, not only will cracks in major crash parts be prevented, but an equivalent level of crash safety performance can be secured.

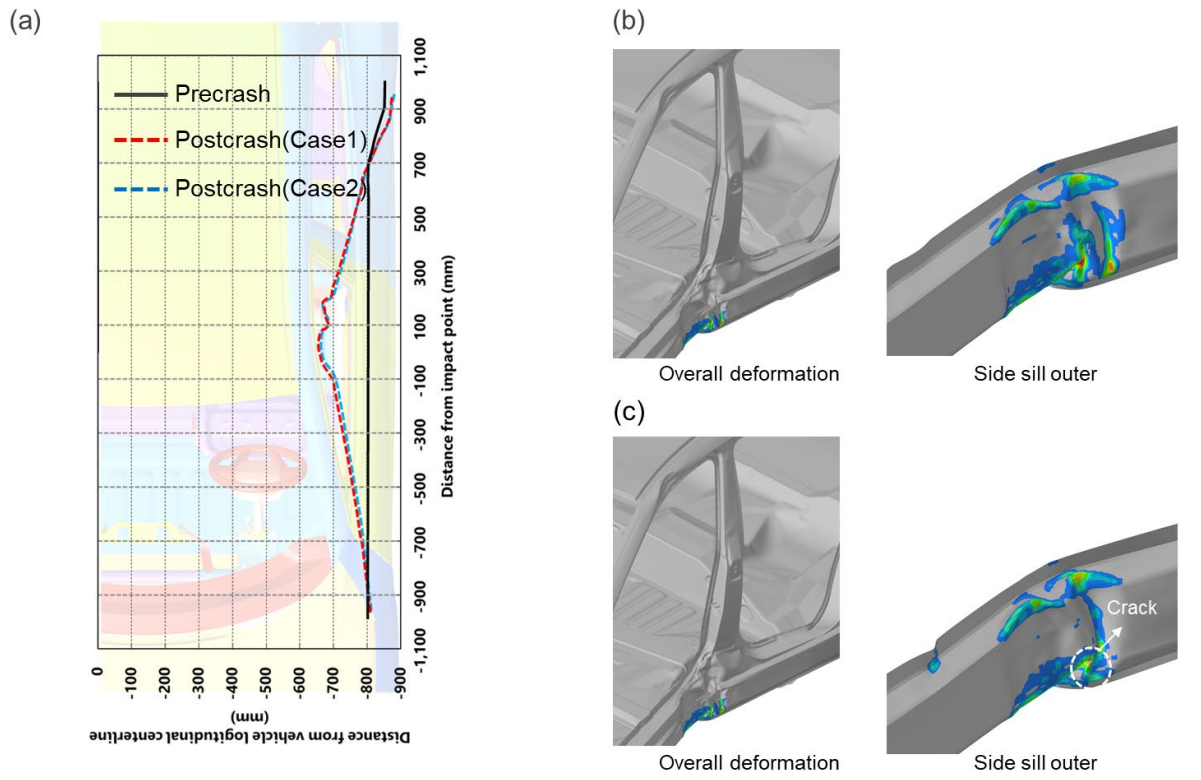

Fig.14: CAE analysis result of side pole crash. (a) Crash profile of side sill outer (b) Side sill deformation(Case1) (c) Side sill deformation(Case2)

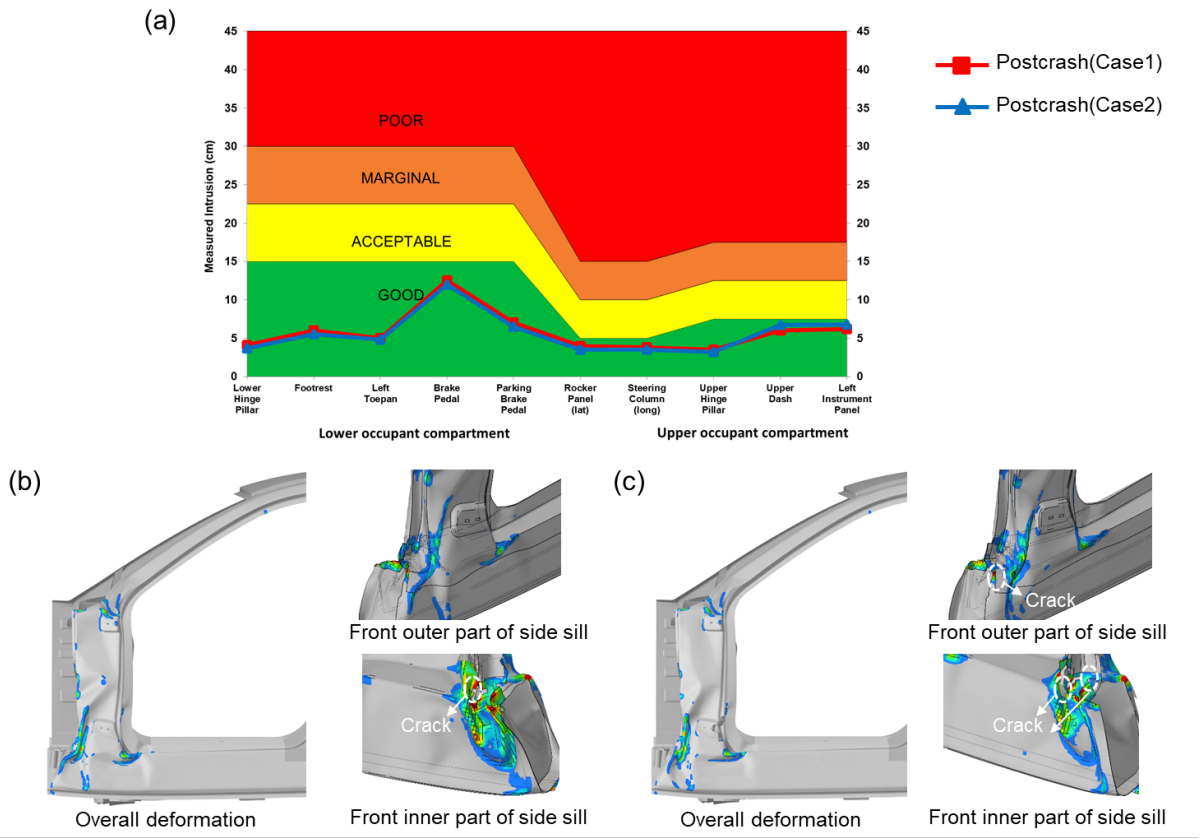

Fig.15: CAE analysis result of small overlap front crash. (a) intrusion result (b) A-Pillar and Side sill deformation(Case1) (c) A-Pillar and Side sill deformation(Case2)

6 Summary and conclusion

Efficient calculation and verification process with user-interface program for crash material card definition was suggested, and following conclusions were drawn by the verification.

1) The efficient process with developed conversion program is applied in the material crash property definition and CAE verification process.

2) With efficient process, able to obtain the good reliability of crash material cards for AHSS & UHSS.

3) Thanks to the standardized calculation method, optimal material parameters for crash property definition can be derived with minimized error caused by manual user calculation.

4) Able to confirm the excellent crash performance for 3 representative steel grades, 1.5GPa PHS type1, 1.5GPa PHS type2 and 1.0GPa CR.

5) Derived crash material card successfully applicate to the Full vehicle crash model and make a comparable result for each steel grades

7 Literature

[1] G. Huang et al, “Fracture characterization of AHSS using two different experimental methods”, 2018 IOP Conf. Ser.: Mater. Sci. Eng. 418 012080

[2] Noder, J., Gutierrez, J., Zhumagulov, A., Khameneh, F. et al., "Constitutive, Formability, and Fracture Characterization of 3rd Gen AHSS with an Ultimate Tensile Strength of 1180 MPa," SAE Int. J. Adv. & Curr. Prac. in Mobility 3(3):1395-1407, 2021

[3] P. Larour, A.Baumer, K.Dahmen, W. Bleck., "Influence of Strain Rate, Temperature, Plastic Strain and Microstructure on the Strain Rate Sensitivity of Automotive Sheet Steels, " steel research int. 84 (2013) No. 5

[4] Bai, Y., Wierzbicki, T. Application of extended Mohr–Coulomb criterion to ductile fracture. Int J Fract 161, 1–20 (2010)

[5] Andrade, F.X.C., Feucht, M., Haufe, A. et al. An incremental stress state dependent damage model for ductile failure prediction. Int J Fract 200, 127–150 (2016).

[6] Heibel, S., Nester, W., Clausmeyer, T. and Tekkaya A.E., “Failure assessment in sheet metal forming using a phenomenological damage model and fracture criterion: experiments, parameter identification and validation,” Procedia Engineering 207 (2017) 2066-2071

[7] Chen, X., Chen, G., Huang.L and Ming F.S, “Calibration of GISSMO Model for Fracture Prediction of A Super High Formable Advanced High Strength Steel,” 15th International LS-DYNA Users Conference, 2018

[8] Anderson, D., Butcher, C., Pathak, N. and Worswick, M.J., “Failure parameter identification and validation for a dual-phase 780 steel sheet,” International Journal of Solids and Structures 124 (2017) 89-107

[9] MJ Worswick, A.Abedini, M.Nemcko, et al., “Dynamic Considerations in Prediction of Fracture of Ultra High-Strength Steel During Crash,” GDIS 2018

[10] Mohr, D. and Marcadet, S., “Micromechanically-motivated phenomenological Hosford-Coulomb model for predicting ductile fracture initiation at low stress triaxialities,” International Journal of Solids and Structures 67-68 (2015) 40-55